

Optimal Quantum Control Using Randomized Benchmarking

J. Kelly,¹ R. Barends,¹ B. Campbell,¹ Y. Chen,¹ Z. Chen,¹ B. Chiaro,¹ A. Dunsworth,¹ A. G. Fowler,^{1,2} I.-C. Hoi,¹ E. Jeffrey,¹ A. Megrant,¹ J. Mutus,¹ C. Neill,¹ P. J. J. O'Malley,¹ C. Quintana,¹ P. Roushan,¹ D. Sank,¹ A. Vainsencher,¹ J. Wenner,¹ T. C. White,¹ A. N. Cleland,¹ and John M. Martinis¹

¹*Department of Physics, University of California, Santa Barbara, California 93106, USA*

²*Centre for Quantum Computation and Communication Technology, School of Physics, The University of Melbourne, Victoria 3010, Australia*

(Received 11 March 2014; published 20 June 2014)

We present a method for optimizing quantum control in experimental systems, using a subset of randomized benchmarking measurements to rapidly infer error. This is demonstrated to improve single- and two-qubit gates, minimize gate bleedthrough, where a gate mechanism can cause errors on subsequent gates, and identify control crosstalk in superconducting qubits. This method is able to correct parameters so that control errors no longer dominate and is suitable for automated and closed-loop optimization of experimental systems.

DOI: 10.1103/PhysRevLett.112.240504

PACS numbers: 03.67.Ac, 03.67.Lx, 85.25.Hv

Quantum information is stored in continuous amplitudes and phases, so quantum control must be precise to achieve the desired state [1]. Achieving control with high fidelity lies at the heart of enabling fault-tolerant quantum computing [2,3]. With gate fidelities approaching the fault-tolerant threshold [4–6], characterizing and reducing the remnant error becomes increasingly challenging. Quantum process tomography can completely characterize a gate, decomposing a process into Pauli or Kraus operators [7,8]. However, improving gates is complicated: gate parameters map nonintuitively onto the process matrix, and state preparation and measurement errors (SPAM) can be confused with process errors.

Here, we present a different approach to achieve high fidelity gates. We use Clifford-based randomized benchmarking (RB) [9,10] to map gate errors onto control parameters, and feed this back to optimize gates. The method is fast and scales to arbitrary precision as the sensitivity to fractional error is independent of gate fidelity [11]; tuning up even higher fidelity gates should be possible. We apply it to general quantum control problems, such as gate optimization, gate bleedthrough [12] and crosstalk. In particular, we demonstrate closed-loop optimization with nonorthogonal parameters in a real, noisy quantum system. As RB is platform independent, our approach is in principle applicable to a variety of quantum systems.

In standard RB, gates are characterized by measuring the fidelities of sequences with varying lengths. We experimentally show that optimizing the *sequence* fidelity at fixed length improves the *gate* fidelity. We call this approach—using the sequence fidelity from randomized benchmarking as a fitness metric for gate performance—optimized randomized benchmarking for immediate tune-up (ORBIT).

As a testbed, we use a five qubit (Q_0 - Q_4) superconducting system [11] based on the Xmon transmon design [13]. Here, XY control is achieved with microwave pulses and Z control with dc current pulses which modulate the qubit frequency. Qubits are coupled capacitively. Qubit frequencies are tuned between $f_{10} = 4$ and 6 GHz, and qubit nonlinearities $\Delta/2\pi$ are around -220 MHz. We use a dispersive readout scheme with a wide band parametric amplifier [14] for state discrimination. This device is an ideal platform for optimizing for small errors, as we have obtained high fidelity single- and two-qubit gates on this device (see Ref. [5,11] for details on device and setup). We use the same device here.

We start with a simple test case where we optimize a single-qubit 90-degree rotation about the X axis in the Bloch sphere representation ($X/2$ gate). This gate is implemented by a microwave pulse with a cosine envelope (Fig. 1(a) inset) centered around frequency f with amplitude A . As the Xmon transmon qubit is a multilevel system, we apply a quadrature correction term with DRAG coefficient α to minimize leakage to higher levels [15–17]. First, we determine the gate fidelity using RB, then measure how control errors affect the fidelity of sequences.

In Clifford-based RB, random Clifford rotations are inserted between the gate under test to ensure that it is applied to a representative set of states. The single-qubit Clifford gates are the group of rotations that map between the two polar and four equally spaced equator states on the Bloch sphere, and are able to generate a sufficient set of states to remove bias from gate error. To quantify the $X/2$ fidelity, we first measure a reference curve by applying many sequences of random Cliffords, appended by recovery Cliffords C_r that make the ideal operation the identity. As we initialize the qubit in the ground state, the ground state population becomes the sequence fidelity. Randomization makes the sequence fidelity follow an exponential decay from the accumulation

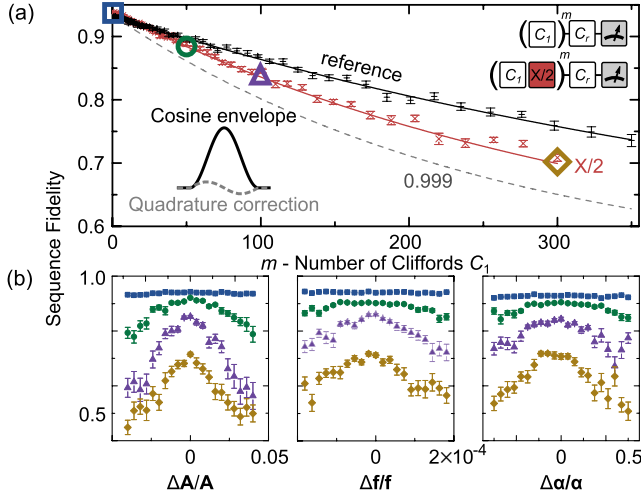


FIG. 1 (color online). (a) Single qubit randomized benchmarking ($k = 40$) for Q_2 at $f_{10} = 5.5223$ GHz. The reference experiment uses sequences of random Cliffords only (black plus); an $X/2$ gate is tested by interleaving it with random Cliffords (red x). The $X/2$ gate has a cosine envelope pulse shape and quadrature correction (inset). (b) Sequence fidelities versus parameters: the pulse amplitude A , frequency f , and coefficient α ($k = 20$). The sequences are measured at $m = 1$ (square), 50 (circle), 100 (triangle), and 300 (diamond).

of gate-specific errors as $Ap_{\text{ref}}^m + B$, with gate errors captured in the characteristic scale p_{ref} [see Fig. 1(a)]. The SPAM errors affect A and B , but not the rate of the decay. Individual gate fidelities are evaluated by interleaving a specific gate between Cliffords, generating a decay curve with scale p_{gate} . By subtracting away the reference curve, we get the gate error $r_{\text{gate}} = (1 - p_{\text{gate}}/p_{\text{ref}})(d - 1)/d$ [18], with $d = 2^n$ a function of the number of qubits n ; here $n = 1$. Each point in m is an average of the fidelity of k different random sequences. We find the fidelity of this $X/2$ gate to be 0.9995 ($k = 40$).

For the data in Fig. 1(b), we set $m = 1, 50, 100, 300$ and measure the sequence fidelity as we vary each of the gate parameters from their optimum. As expected, we find that longer length sequences drop more rapidly in fidelity away from the maximum, indicating an increased sensitivity to gate error with sequence length. It is this feature that opens a viable route to optimizing arbitrarily high fidelity gates: sensitivity can be maintained by doubling m when the error is halved [11].

In the rest of this Letter, we demonstrate that ORBIT is applicable to a variety of nontrivial parametrized tune-up problems, such as entangling gate optimization with non-orthogonal parameters, improving waveform control for reducing gate bleedthrough, and minimizing crosstalk in a multiqubit system. We emphasize that these applications are issues of prime importance to high fidelity and scaling up to larger qubit systems [19].

We start by applying ORBIT to a controlled-phase (CZ) entangling gate with qubits Q_2 and Q_3 that have

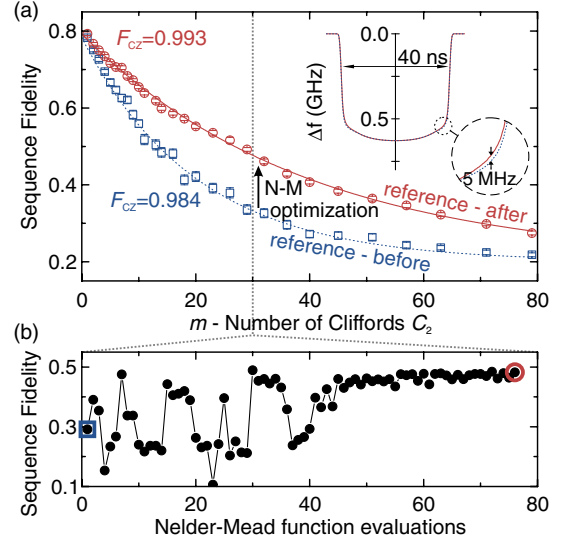


FIG. 2 (color online). Optimizing the fidelity of a two-qubit CZ gate. (inset a) One qubit undergoes an effective adiabatic trajectory in frequency that brings the $|11\rangle$ and $|02\rangle$ near resonance, producing a conditional phase. Q_2 idles at $f_{10} = 5.5223$ GHz, and Q_3 idles at $f_{10} = 4.6639$ GHz. (a) The sequence fidelity of the reference curve versus number of two-qubit Cliffords before (blue squares) and after (red circles) optimization ($k = 50$). This optimization has shifted the shoulder of the trajectory by up to 5 MHz (inset). (b) The change in sequence fidelity at $m = 30$ versus Nelder-Mead function evaluations ($k = 20$), starting at a fidelity of 0.3 (blue square), and converging on a sequence fidelity of 0.5 (red circle). The fidelity of the CZ improved from $F_{\text{CZ}} = 0.984$ to $F_{\text{CZ}} = 0.993$, measured using interleaved RB [11].

$g/2\pi = 30$ MHz coupling, as described in Ref. [5,20]. With the addition of many nonorthogonal gate parameters and a larger Hilbert space, this is a significant increase in complexity compared to the $X/2$ gate. The CZ gate is performed by moving a qubit along an adiabatic trajectory in frequency [20] [see inset Fig. 2(a)] which brings the $|11\rangle$ and $|02\rangle$ avoided level crossing near resonance, generating a conditional phase. The fidelity of this gate is sensitive to the frequency trajectory, as deviations from the ideal can cause a conditional phase other than π as well as non-adiabatic leakage errors to $|02\rangle$. The gate depends on eight parameters that follow straightforwardly from theory (see Ref. [20]).

The direct mapping that ORBIT provides between the control parameters and gate fidelity allows for automated optimization. Here, we used the Nelder-Mead algorithm for closed-loop control [21]. As a metric, we use sequences ($m = 30$) composed of gates from the two-qubit Clifford group C_2 , generated with an average of 8.25 single-qubit gates and 1.5 CZ gates per Clifford [5]. As single-qubit gates have a substantially higher fidelity, the CZ error is a significant contribution to the Clifford error, making the reference fidelity a metric for CZ gate fidelity. Figure 2(a) shows the reference curves before (blue squares) and after

(red circles) optimization. The average error per Clifford was reduced from $r = 0.0361$ to $r = 0.0188$. Taking into account the average number of single and CZ gates in a two-qubit Clifford, these values are consistent with a CZ gate fidelity improvement from 0.984 to 0.993 (see Ref. [11] for interleaved data). Figure 2(b) shows the evolution of the sequence fidelity versus number of evaluations, starting with the blue square; it initially varies strongly with small parameter changes, underlining the sensitivity of this method, and eventually converges on optimal parameters (red circle). The inset of Fig. 2(a) shows the small change in waveform shape (up to 5 MHz in magnitude) that improves fidelity.

Figure 2 illustrates the advantages of this approach. First, we can identify and remedy small errors in an environment with noise; we optimize parameters to where gate errors are no longer dominated by control imperfections (see Ref. [5] for a representative error budget for a similar experiment). Second, our approach is fast: the total number of measurements is 18000 ($k = 20$ sequences, 900 repetitions each), which can be performed in 2 seconds with our system. Third, the optimization is model free, which is a powerful tool as the system Hamiltonian is not always known to high precision. We believe this will be critical to improving gates beyond current fidelities.

We have used the Nelder-Mead algorithm with ORBIT for automated tune-up as it is a gradient-free method, and therefore less sensitive to noise. While here we used Nelder-Mead for “last-mile” optimization—where gate parameters are initially near the global optimum—any algorithm which uses a fitness metric could be used with ORBIT. Possible applications lie in implementing model-free gates, such as with numerical optimal control [22,23], where pulses are discretized into pixels. This technique can be used on the full Hamiltonian without approximation, can optimize for robustness against noise or experimental parameters, and can generate gates as fast as the “quantum speed limit” [24]. Experimentally implementing such gates is hindered by differences between the modeled and actual system Hamiltonians. ORBIT could be a bridge by providing a fitness metric for the closed-loop approaches such as *ad hoc* (see Ref. [25]).

We now use ORBIT to minimize gate bleedthrough; this is a particularly harmful problem because it causes gate-specific errors on potentially many subsequent gates. Gate bleedthrough occurs when the mechanism for implementing a gate is not adequately turned off at the end. Physical mechanisms include reflections of control pulses, stray inductance in control lines, and amplifier slew rates for microwave systems. Gate bleedthrough is challenging to characterize and correct, because the entire time domain response must be optimized. Here, we demonstrate that ORBIT is sensitive to a gate bleedthrough mechanism, allowing for optimization.

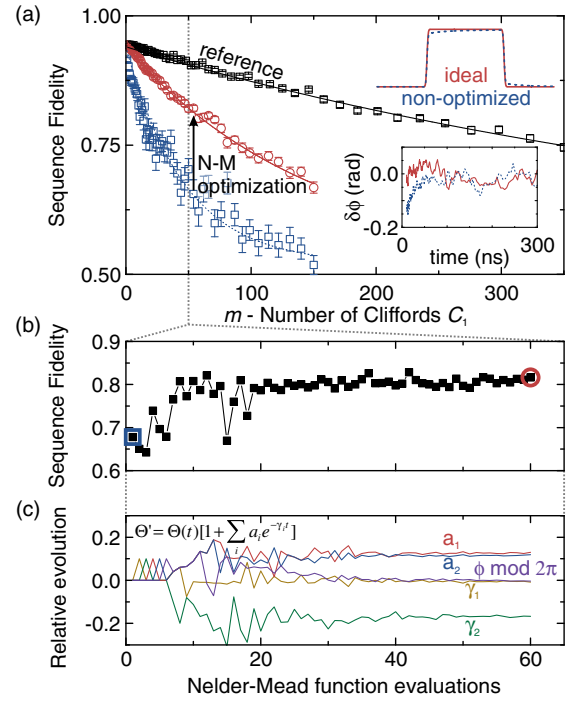


FIG. 3 (color online). Reducing gate bleedthrough. (top inset a) For rotating the state around the Z axis (Bloch sphere representation), the qubit frequency is detuned by a step pulse, with $t_{\text{gate}} = 35$ ns and large frequency change $\Delta f = -0.37$ GHz which is ideally flat (solid red). Nonidealities in control and wiring bring about a nontrivial deformation of the waveform (dashed blue), causing gate bleedthrough. (a) Sequence fidelity vs number of Cliffords for the reference (black squares), and interleaved with the step pulse for Q_2 at $f_{10} = 5.5223$ GHz. The error per Clifford plus step pulse is reduced using ORBIT from $r = 0.011$ (blue squares) to $r = 0.003$ (red circles). With this improvement, the remnant qubit phase $\delta\phi(t)$ after the step pulse is notably more flat (bottom inset), determined via quantum state tomography ($k = 40$). (b) Sequence fidelity during the Nelder-Mead algorithm ($k = 30$). (c) Evolution of transfer function parameters, written in terms of the step response Θ' .

We reduce gate bleedthrough from a detune operation which is implemented using a square step pulse on the qubit frequency control line of Q_2 . The qubit is detuned for 35 ns by -0.37 GHz, acquiring a single-qubit phase $\phi = 13.2\pi$. These current pulses can detune the qubit during subsequent gates if not properly leveled, as illustrated in the top inset of Fig. 3(a). In the bottom inset, we measure deviations $\delta\phi(t)$ from the ideal acquired qubit phase before and after correction. We compensate the waveform for stray inductances and reflections in the line by applying an inverse transfer function with two poles, expressed in terms of the step response: $\Theta'(t) = \Theta(t)[1 + \sum_i a_i \exp(-\gamma_i t)]$, with $\Theta(t)$ the Heaviside step function, and amplitudes a_i and rates γ_i . In Fig. 3(a), the error of a Clifford plus step pulse is reduced from $r = 0.011$ to $r = 0.003$ by Nelder-Mead optimization. The sequence fidelity and evolution of the parameters a_i , γ_i , and accumulated qubit phase are

shown to converge in Fig. 3(b) and Fig. 3(c). Gate bleedthrough is reduced as evidenced in the improved sequence fidelity. Additionally, the remnant qubit phase $\delta\phi(t)$ is markedly flatter after the detuning pulse as the variance in phase is reduced from 22×10^{-4} to 8×10^{-4} rad² [see the bottom inset of Fig. 3(a)]. This demonstrates that gate bleedthrough—here arising from imperfect zeroing of Z control—can be minimized without the need for a full time-domain characterization.

We also apply ORBIT to optimization problems relevant to large systems. One of the greatest challenges in scaling up to larger quantum systems is to maintain addressability over single qubits as control pulses for one qubit can affect others. In our architecture, we minimize control crosstalk by alternating the qubit frequency [13]; next-nearest neighbors however are prone to crosstalk due to the smaller frequency difference [see Fig. 4(a)]. A difficulty in minimizing crosstalk lies in characterizing its effect on gates. Here, ORBIT provides an elegant solution by mapping errors onto the relevant parameters, through the isolated and simultaneous application of single-qubit Cliffords [26].

We start by measuring the reference fidelity curve for qubit labeled Q_2 , shown in Fig. 4(b). From the decay, we find an average error per Clifford of $r_c = 0.001$, consistent with the average single-qubit gate fidelity of $F = 0.9995$.

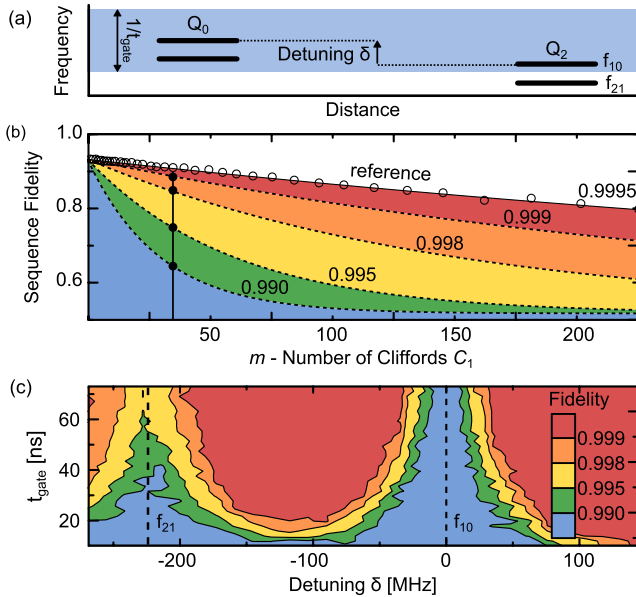


FIG. 4 (Color online) (color online). Mapping control crosstalk. (a) Energy level diagram of the qubits Q_2 and Q_0 . Control pulses are applied to the XY lines of Q_2 and Q_0 ; the latter is swept in detuning δ and gate length t_{gate} . Control crosstalk can be exacerbated by small detunings or fast gates. (b) Single-qubit benchmarking of Q_2 at $f_{10} = 5.5223$ GHz. The colored regions indicate different ranges of reference fidelity. The vertical cut indicates the m value used to discriminate between regions. (c) The inferred gate fidelity ($m = 35$, $k = 20$) versus detuning and gate length [11].

The colored regions indicate different ranges in reference fidelity; we use this as a map to infer the gate fidelity from the sequence fidelity. Next, we monitor the sequence fidelity (with $m = 35$) of Q_2 while sending pulses for single-qubit Cliffords down the control line of Q_0 . We can ignore the state of Q_0 . We vary both the detuning δ and gate length t_{gate} for pulses on the Q_0 line, while keeping the product of gate length and amplitude fixed to mimic control crosstalk. The inferred gate fidelity of qubit Q_2 is shown in Fig. 4(c). The red regions indicate minimal added error from crosstalk ($< 0.05\%$), while the blue regions show significant increase in error ($> 1\%$). Clear signatures of infidelity appear when crosstalk signals are resonant with the qubit transition frequencies f_{10} or f_{21} , as illustrated in blue in Fig. 4(a), and fall off with detuning and gate length as expected.

The data in Fig. 4 demonstrate that ORBIT can provide a map to visualize and optimize control crosstalk in a straightforward manner, without the need to characterize or recalibrate the pulses on qubit Q_0 . This technique could in principle also be used for crosstalk reduction methods that reduce spectral power at overlapping frequencies (see Ref. [27,28]).

In using ORBIT, we explicitly assume that the cause of sequence decay remains unchanged: the single exponential decay, and SPAM errors captured in parameters A and B , must be consistent. We experimentally find that behavior remains consistent, by comparing standard RB before and after optimization (Fig. 2 and Fig. 3). This consistency and stable fidelities over many hours suggest that drifts in qubit and control parameters are small. In addition, leakage out of the computational subspace is assumed to penalize sequence fidelity [29]. The results show that small leakage errors penalize fidelity for single- and two-qubit gates (Fig. 1(b), Fig. 2). Interestingly, while RB assumes that gate errors are independent of previous gates and Cliffords fully randomize over the computational subspace, we are able to minimize gate bleedthrough and leakage. Clearly, more work needs to be done to fully understand the limitations and capabilities of Clifford-based RB. Because of these subtleties, we emphasize that the reference and interleaved RB data always should be verified for self-consistency [5,11].

We have experimentally tested a new approach for optimizing quantum control using randomized benchmarking. This has been shown to be effective for improving single- and two-qubit gates, minimizing gate bleedthrough, and identifying control crosstalk. These experiments are a representative set of control problems for realizing high fidelity gates on large quantum systems. We believe ORBIT can be a generic tool for implementing closed-loop optimization in experimental systems, due to its speed, accuracy and platform independence.

We thank F. Wilhelm and D. Egger for helpful discussions on gate optimization and the Nelder-Mead algorithm. We also thank A. N. Korotkov and A. Veitia for help

in implementing Clifford-based RB. This work was supported by the Office of the Director of National Intelligence (ODNI), Intelligence Advanced Research Projects Activity (IARPA), through the Army Research Office Grants No. W911NF-09-1-0375 and No. W911NF-10-1-0334. All statements of fact, opinion, or conclusions contained herein are those of the authors and should not be construed as representing the official views or policies of IARPA, the ODNI, or the U.S. Government. Devices were made at the UC Santa Barbara Nanofabrication Facility, a part of the NSF-funded National Nanotechnology Infrastructure Network, and at the NanoStructures Cleanroom Facility. J. Kelly and R. Barends contributed equally to this work.

-
- [1] M. Shapiro and P. Brumer, *Principles of the Quantum Control of Molecular Processes* (Wiley, New York, 2003), p. 250.
- [2] M. A. Nielsen and I. L. Chuang, *Quantum Computation and Quantum Information* (Cambridge University Press, Cambridge, England, 2010).
- [3] A. G. Fowler, M. Mariantoni, J. M. Martinis, and A. N. Cleland, *Phys. Rev. A* **86**, 032324 (2012).
- [4] J. Benhelm, G. Kirchmair, C. F. Roos, and R. Blatt, *Nat. Phys.* **4**, 463 (2008).
- [5] R. Barends, J. Kelly, A. Megrant, A. Veitia, D. Sank, E. Jeffrey, T. White, J. Mutus, A. Fowler, B. Campbell *et al.*, *Nature (London)* **508**, 500 (2014).
- [6] K. R. Brown, A. C. Wilson, Y. Colombe, C. Ospelkaus, A. M. Meier, E. Knill, D. Leibfried, and D. J. Wineland, *Phys. Rev. A* **84**, 030303 (2011).
- [7] J. L. O'Brien, G. J. Pryde, A. Gilchrist, D. F. V. James, N. K. Langford, T. C. Ralph, and A. G. White, *Phys. Rev. Lett.* **93**, 080502 (2004).
- [8] T. Yamamoto, M. Neeley, E. Lucero, R. Bialczak, J. Kelly, M. Lenander, M. Mariantoni, A. OConnell, D. Sank, H. Wang *et al.*, *Phys. Rev. B* **82**, 184515 (2010).
- [9] E. Magesan, J. Gambetta, and J. M. Emerson, *Phys. Rev. Lett.* **106**, 180504 (2011).
- [10] A. D. Córcoles, J. M. Gambetta, J. M. Chow, J. A. Smolin, M. Ware, J. Strand, B. L. T. Plourde, and M. Steffen, *Phys. Rev. A* **87**, 030301 (2013).
- [11] See Supplemental Material <http://link.aps.org/supplemental/10.1103/PhysRevLett.112.240504> for discussion of ORBIT scaling with fidelity and additional data for Figs. 3 and 4.
- [12] S. Gustavsson, O. Zwiernik, J. Bylander, F. Yan, F. Yoshihara, Y. Nakamura, T. P. Orlando, and W. D. Oliver, *Phys. Rev. Lett.* **110**, 040502 (2013).
- [13] R. Barends, J. Kelly, A. Megrant, D. Sank, E. Jeffrey, Y. Chen, Y. Yin, B. Chiaro, J. Mutus, C. Neill *et al.*, *Phys. Rev. Lett.* **111**, 080502 (2013).
- [14] J. Mutus, T. White, R. Barends, Y. Chen, Z. Chen, B. Chiaro, A. Dunsworth, E. Jeffrey, J. Kelly, A. Megrant *et al.*, [arXiv:1401.3799](https://arxiv.org/abs/1401.3799).
- [15] F. Motzoi, J. M. Gambetta, P. Rebentrost, and F. K. Wilhelm, *Phys. Rev. Lett.* **103**, 110501 (2009).
- [16] E. Lucero, J. Kelly, R. C. Bialczak, M. Lenander, M. Mariantoni, M. Neeley, A. OConnell, D. Sank, H. Wang, M. Weides *et al.*, *Phys. Rev. A* **82**, 042339 (2010).
- [17] J. M. Chow, L. DiCarlo, J. M. Gambetta, F. Motzoi, L. Frunzio, S. M. Girvin, and R. J. Schoelkopf, *Phys. Rev. A* **82**, 040305 (2010).
- [18] E. Magesan, J. M. Gambetta, B. Johnson, C. A. Ryan, J. M. Chow, S. T. Merkel, M. P. da Silva, G. A. Keefe, M. B. Rothwell, T. A. Ohki *et al.*, *Phys. Rev. Lett.* **109**, 080505 (2012).
- [19] A. G. Fowler, *Phys. Rev. A* **89**, 032316 (2014).
- [20] J. M. Martinis and M. R. Geller, [arXiv:1402.5467](https://arxiv.org/abs/1402.5467).
- [21] R. S. Judson and H. Rabitz, *Phys. Rev. Lett.* **68**, 1500 (1992).
- [22] N. Khaneja, T. Reiss, C. Kehlet, T. Schulte-Herbrüggen, and S. J. Glaser, *J. Magn. Reson.* **172**, 296 (2005).
- [23] D. Egger and F. Wilhelm, *Supercond. Sci. Technol.* **27**, 014001 (2014).
- [24] T. Caneva, M. Murphy, T. Calarco, R. Fazio, S. Montangero, V. Giovannetti, and G. E. Santoro, *Phys. Rev. Lett.* **103**, 240501 (2009).
- [25] D. Egger and F. K. Wilhelm, *Phys. Rev. Lett.* **112**, 240503 (2014).
- [26] J. M. Gambetta, A. Córcoles, S. Merkel, B. Johnson, J. A. Smolin, J. M. Chow, C. A. Ryan, C. Rigetti, S. Poletto, T. A. Ohki *et al.*, *Phys. Rev. Lett.* **109**, 240504 (2012).
- [27] R. Schutjens, F. A. Dagga, D. J. Egger, and F. K. Wilhelm, *Phys. Rev. A* **88**, 052330 (2013).
- [28] V. Vesterinen, O.-P. Saira, A. Bruno, and L. DiCarlo, [arXiv:1405.0450](https://arxiv.org/abs/1405.0450).
- [29] J. M. Epstein, A. W. Cross, E. Magesan, and J. M. Gambetta, [arXiv:1308.2928](https://arxiv.org/abs/1308.2928).